# Continuum-Legged Biped with a Kangaroo-Inspired Tail for Tripedal Locomotion: Preliminary Design and Validations

Gavin Platt[1], Ian Walker[2], *IEEE Fellow*, and Ge Lv[1], *IEEE Member*

***Abstract*— This paper presents the design and preliminary validation of a compliant continuum-legged biped robot equipped with a kangaroo-inspired tail for enhanced stability and adaptability. In contrast to using legs based on traditional rigid link "vertebrate" designs, the tendon-actuated compliant legs mimic octopus behavior for "invertebrate" bipedal locomotion, in coordination with the tail. The robot uses a hierarchical hybrid control framework to achieve level-ground walking (on different terrain conditions), obstacle avoidance, and push recovery under perturbations. Experimental results demonstrate stable walking with rhythmic tail load transfer over different terrain conditions, effective turning and object avoidance, and recovery from external force perturbations. Three sets of experiments were conducted to validate the prototype's performance. These results demonstrate the potential of combining continuum limbs with an actively controlled tail to enhance balance robustness and locomotion versatility in hybrid soft-rigid robots.**

## I. Introduction

Achieving both stability and versatility in legged robotic locomotion remains challenging [1]–[3]. Biomechanics-inspired compliance can improve both by attenuating impacts, shaping stance dynamics, and enabling energy storage/return [4]. This has motivated designs that incorporate elasticity in the leg or actuation chain (e.g., series elastic actuation) to achieve low-impedance interaction and robustness to impulsive loads [5], as well as passive-dynamic and hybrid walkers where tuned compliance reduces feedback burden while preserving gait robustness [6]. However, most prior platforms rely on rigid-link legs with compliance localized at joints (e.g., ankle). Here, we instead consider continuum legs and evaluate whether distributed elasticity can enable task-adaptive locomotion for relatively high-mass, high-inertia platforms [7], [8].

We take inspiration from behaviors observed in octopus and kangaroo locomotion. Several species of octopus have been known to exhibit a bipedal gait while moving across the ocean floor. Rather than swimming or using all eight appendages for crawling, amphioctopus marginatus and abdopus aculeatus [9], [10], and (most recently discovered) octopus vulgaris [11] were observed to propel themselves forward by using their (inherently compliant) posterior arms functionally as legs in bipedal locomotion, thus keeping their remaining arms free for camouflage or defense. This behavior represents an interesting "existence proof" of bipedal locomotion using compliant continuous backbone "continuum" limbs.

Bipedal octopus locomotion is inherently supported in part by the animal's neutral or semi-neutral buoyancy, which under the water aids in counteracting gravity. For out of water locomotion, the focus of this paper, counteracting gravity is a greater challenge for continuum legs, particularly for robots with relatively large and/or massive bodies.

To address this issue, our work is further inspired by the locomotion of kangaroos. When walking in low-ceilinged or confined spaces, kangaroos will initiate a pentapedal walking gait whereas their tails are used as a fifth point of contact as shown in Fig. 1 [12]. This strategic placement of the tail stabilizes the kangaroo and propels it forward. In [13] the authors provide evidence that during slow gait kangaroo walking there is a tail repositioning phase in which the tail is repositioned before the kangaroo lifts its hind legs. This repositioning is what affords the kangaroo its stability and propulsion. Dawson et al. [14] detail the muscular anatomy of the Macropus fuliginosus and show how its tail forms a triped between the tail and forelimbs as it is swinging its hindlimbs forward in a pentapedal gait.

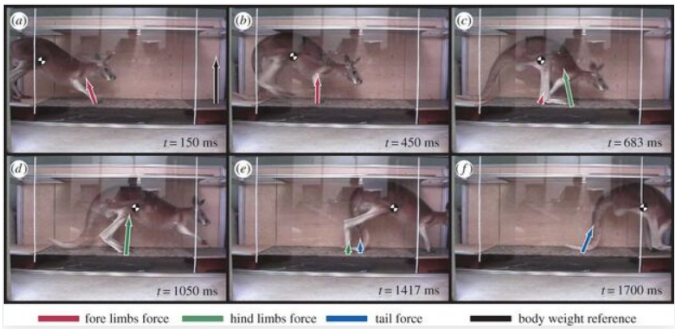


Fig. 1. This figure observes a montage of a kangaroo exhibiting pentapedal motion (a-f) during confined space movement, where the kangaroo's tail propels and powers pentapedal locomotion. The forces in motion are illustrated. Reproduced from O'Connor et al. [12], Biology Letters, 10(7): 20140381. © The Royal Society.

Bipedal octopus locomotion provides inspiration for compliant legs, while kangaroo behavior demonstrates how an active tail can function as a dynamic load bearing limb. Combining these strategically advantageous features, the robot introduced in this paper aims to achieve both terrain adaptability and stability during stepping using a continuum legged biped equipped with an active tail.

There has been some previous work in terrestrial continuum-legged locomotion. Godage et al. introduced a

*This work was supported by the CECAS Undergraduate Research Grant of Clemson University.

[1]Gavin Platt and Ge Lv are with the Department of Mechanical Engineering, School of Mechanical and Automotive Engineering, Clemson University, Clemson, SC 29634, USA. {gplatt, glv}@clemson.edu

[2]Ian Walker is with the Department of Electrical Engineering & Computer Science, University of Wyoming, Laramie, WY 82071, USA. iwalker2@uwyo.edu

quadruped with continuum legs capable of crawling and rejecting disturbances [15]. Later work introduced was a triped continuum legged underwater robot [16]. Subsequent related works expanded versatility through reinforcement learning [17], regulating deformation of quadruped continuum legs with closed-loop control [18], and negotiating steep inclines with soft pneumatic continuum hexapod gaits [19]. Advancing fabrication methods and control allowed for navigating unstructured terrain [20] and the development of electronics-free pneumatic circuits generating gaits in soft legged quadrupeds [21]. Other continuum based locomotion strategies include a vacuum-actuated tube capable of climbing [22], a dual spring vacuum tube capable of turning direction while crawling [23], a fully 3D-printed inchworm [24], and omnidirectional capability inspired by caterpillars [25].

The use of tail appendages has been widely investigated as a means of enhancing locomotor stability. Prior studies have demonstrated that actively controlled tails can significantly improve balance and dynamic performance in legged systems. For example, Liu et al. developed a bio-inspired kangaroo robot that leverages an active tail to enhance dynamic stability and locomotion efficiency [26]. Likewise, An et al. proposed a bipedal hopping robot with a maneuverable tail that modulates its moment of inertia in real time to achieve improved balance control [27]. Related work has also explored the use of continuum tail structures to support stability during locomotion [28].

The objective of this research is to investigate the potential and advantages of combining continuum legs with an active tail for locomotion. The following section details the design and control architecture of the robot. Section III describes experiments conducted with the prototype, with the results and analysis of the experiments presented in Section IV. Conclusions are given in Section V.

## II. Design and Prototyping of the Biped

In this section, we describe the major components and the control system of the biped.

### A. Continuum Limbs and Actuators

A view of the biped prototype and its corresponding 3D model are shown in Fig. 2. Each leg is actuated by a lateral roll servo motor at the hip joint, followed by a sagittal-plane pitch servo (hereafter referred to as the leg servo). The leg servo connects to a compliant continuum base that forms the lower limb structure. Each continuum base integrates two tendon-driven servo motors that regulate its deformation (side view in Fig. 3). Specifically, a side servo motor and a frontal servo independently control bending in the frontal and sagittal planes, respectively. By coordinating these two inputs, the continuum leg can achieve smooth bending in any intermediate plane within its workspace. Distally, each continuum leg terminates in an ankle joint that provides frontal-plane motion.

In addition to the legs, the biped is equipped with a tail actuated by a linear actuator, enabling vertical motion in the sagittal plane (Fig. 4). The actuation system comprises four

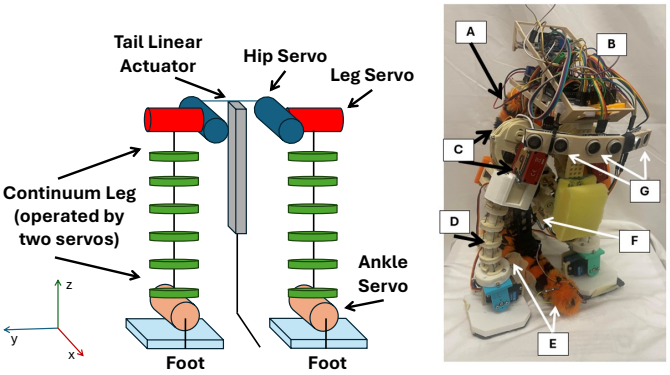


Fig. 2. 3D kinematic model (left) and labeled components of the biped (right). The components are: A) tail linear actuator, B) micro-controller stack, C) tendon-drive servos for the continuum legs, D) continuum legs, E) foot-mounted FSR sensors, F) MPU/Inertial Measurement Unit (IMU) sensor module, and G) ultrasonic distance sensors.

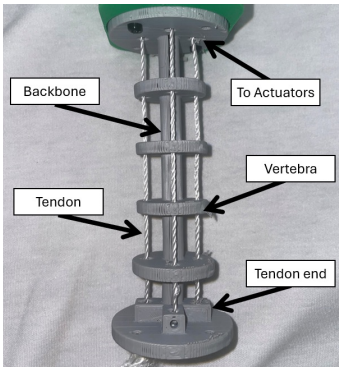


Fig. 3. Labeled components of the continuum leg.

Smraza 45KG servo motors (two assigned to the hip joints and two to the side continuum actuation), two HobbyPark 12KG HD1223MG micro servos for the leg joints, two Betu 70KG TBETU-B70KG-180 servos for the frontal continuum actuation, and two DS3235 35KG high-torque RC servos for the ankle joints.

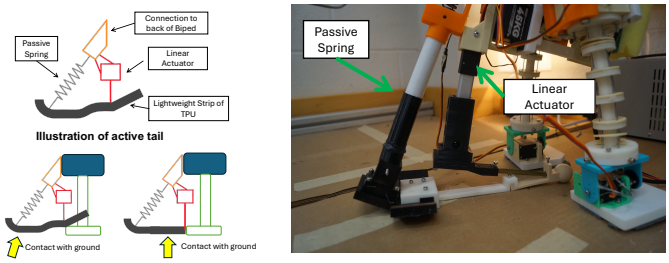


Fig. 4. Schematic and components of the designed tail.

### B. Onboard Sensors

The biped is equipped with a suite of onboard sensors to support task-dependent walking gaits. A primary sensing component is the MPU-6050 motion tracking unit, which integrates a three-axis accelerometer and a three-axis gyroscope. Accelerometer measurements are used to detect

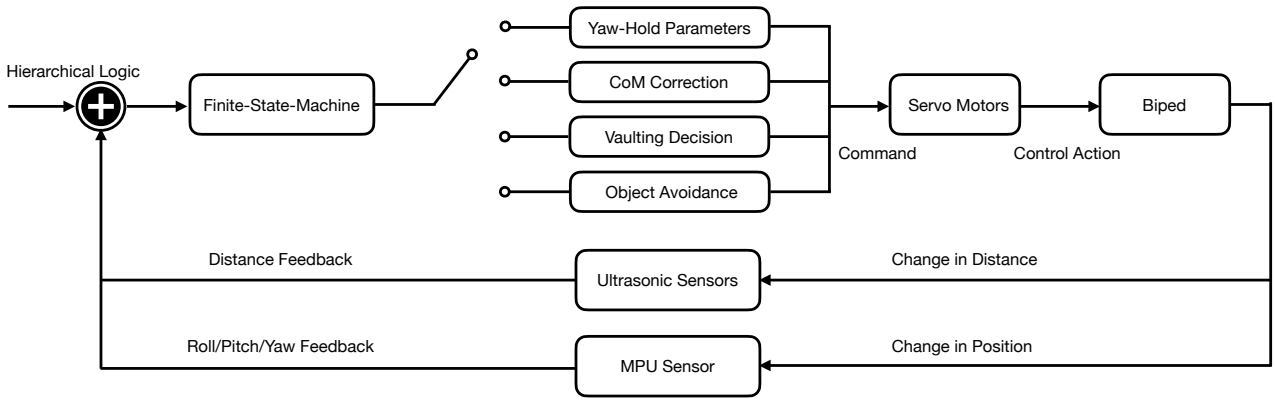


Fig. 5. FSM controller, this diagram showcases how the FSM selects the controller needed and then receives feedback from all sensors.

body motion, while gyroscope outputs, expressed in Euler angles, provide estimates of the biped's orientation. Electrical power consumption is monitored using an ACS712 Hall-effect current sensor and a voltage sensor module, which measure the supplied current and voltage, respectively. To quantify ground interaction forces, two force-sensitive resistors (FSRs) are mounted at the front and rear of the tail to measure reaction forces between the tail and the ground. In addition, the biped is outfitted with three ultrasonic distance sensors (UDSs) that emit ultrasonic pulses and measure the time-of-flight of the reflected signals to estimate distances to nearby objects. For validation and additional experimental evaluation, a BNO080 9-axis IMU is mounted near the biped's center of mass (CoM) to provide independent measurements of body motion and displacement.

### C. Control Architecture

A diagram of the overall control diagram is shown in Fig. 5. We have designed and implemented four different controllers for the biped: 1) straight walking with yaw hold, 2) CoM correction, 3) vaulting reflex, and 4) object avoidance. The overall control system is governed by a hierarchical logic realized through a graphical user interface. Each of the biped's servo motors is controlled with internally closed-loop controllers. Each onboard servo uses an internal closed-loop position controller driven by pulse width modulation commands and feedback from an integrated potentiometer. Once a control mode is enabled, an Arduino-based finite-state machine [29] governs system behaviors. Guard conditions are implemented as inequality checks on sensor signals, while hysteresis bands, debounce counters, and refractory timers are employed to suppress noise-induced false state transitions.

The straight-walking controller with yaw hold regulates the biped's heading to maintain a straight trajectory. When the yaw error exceeds predefined hysteresis bounds, a corrective step is executed on the opposing leg to restore forward alignment. This behavior is governed by a relay (bang-bang) control law. The CoM correction controller is a disturbance-triggered push-recovery reflex that monitors linear acceleration and IMU roll and pitch. Lateral disturbances elicit a counteracting continuum lean and ankle response, while pitch disturbances trigger a forward recovery step to maintain balance. The vaulting reflex is an event-triggered controller [30] that monitors IMU roll during walking. Upon detecting obstacle contact, a vaulting primitive shifts weight, elevates the swing leg, and replants the foot until roll returns to a safe band and the obstacle is cleared. Finally, object avoidance is supervised by a rule-based finite-state machine that monitors three forward-facing UDS. If an obstacle is detected within a threshold distance, the controller initiates repeated left or right turning steps. Turning terminates once a safe distance is restored or a maximum step count is reached, with yaw monitored as a safety guard to prevent excessive rotation.

## III. Experimental Trials

Once the prototyping and initial testing was complete, we conducted a series of testing on the prototype, including level-ground walking with different terrain conditions, navigating obstacles, and maintaining balance under external perturbations.

### A. Straight-Line Walking Trials

The initial walking trial was conducted on level-ground, where the biped was tasked to walk a distance of 30.5 cm in 60 seconds. The screenshots of the initial walking trials are shown in Fig. 6. To further evaluate the biped's ability to overcome unknown and varying terrain, we conducted walking trials with two other terrain conditions: 1) walking with one foot of the biped on faux grass to introduce an uneven surface, and 2) walking with an obstacle placed along the path. The obstacle on the path required the biped to step on and overcome the perturbation. Screenshots of the walking trials are shown in Fig. 7. When walking on the faux grass, the yaw hold controller was initiated. This ensured the biped compensated for the uneven terrain with a stutter step, as needed, to keep the biped moving straight. During obstacle trials, the vaulting reflex controller monitored MPU measurements to detect obstacle contact and initiate the vaulting maneuver.

### B. Navigation and Obstacle Avoidance Trials

The next experiment was conducted for the biped to detect and plan its trajectories to navigate in a confined environment

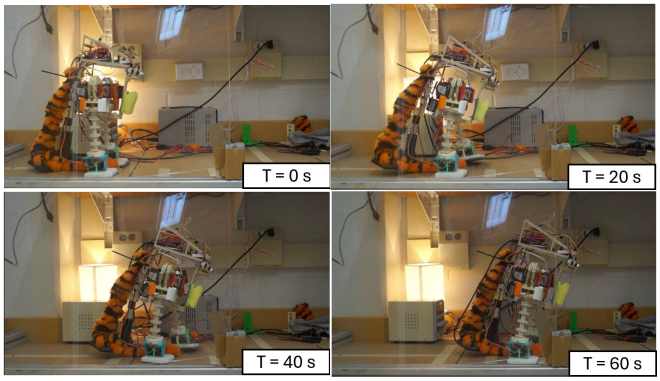


Fig. 6. Screenshots of the biped during level-ground walking.

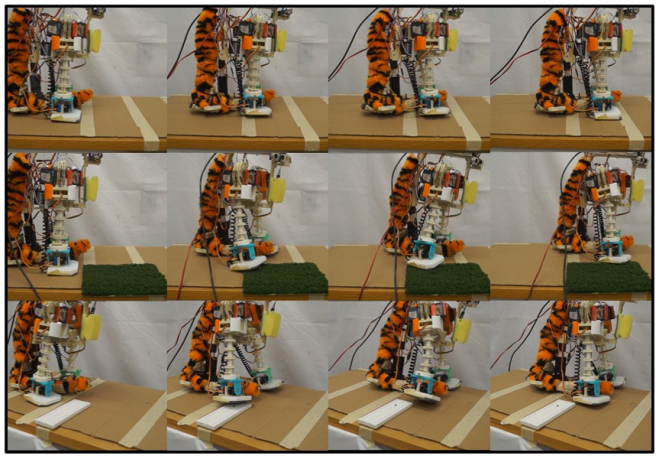

Fig. 7. Montage of straight-line walking trials: bare ground (top), faux grass (middle), and a plastic obstacle (bottom).

using the onboard UDS. We set up two inland barriers and a box as the course for the biped to detect and avoid. Overall, seven trials were conducted, where screenshots of sample trials are shown in Fig. 8. The biped was able to successfully navigate all seven trials without hitting any obstacles.

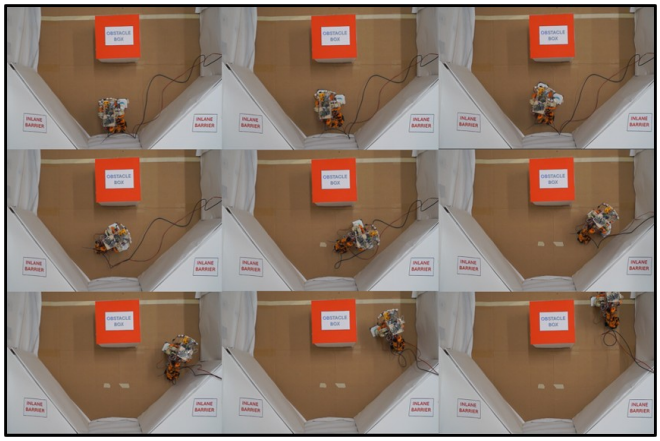

Fig. 8. Screenshots of the biped navigating the course. The biped started at the bottom, and a trial was marked complete with the biped crossing either side of the white finish line (at the top) without hitting the obstacle box.

### C. Push Recovery under External Perturbations

Push recovery experiments were conducted to evaluate the biped's ability to withstand external disturbances applied to the chassis. The experimental protocol follows established methods in [31]. A pendulum-based disturbance apparatus was constructed to deliver controlled impacts under two test conditions. In the first condition, a lateral disturbance was applied by striking the side of the biped with a pendulum mass equal to one quarter of the biped's body weight. In the second condition, the biped was struck from the rear. For each condition, three trials were performed: 1) baseline walking without disturbance, 2) impact without push-recovery control, and 3) impact with push-recovery enabled. The biped's displacement was measured using a BNO080 IMU. During lateral disturbance trials, push-recovery was achieved by activating the side continuum and ankle servos in response to MPU-based disturbance detection. During rear-impact trials, recovery was executed via a forward recovery step triggered by the onboard MPU.

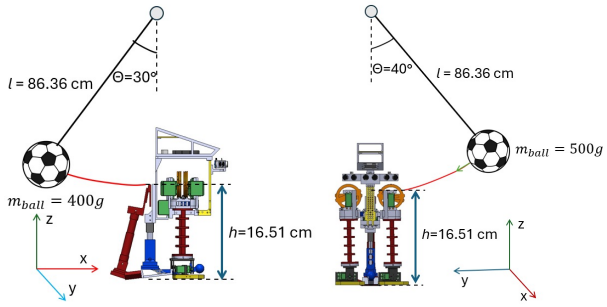


Fig. 9. Illustration of perturbation setup: rear (left) and side (right).

## IV. Results and Discussions

### A. Straight-Line Walking Trials

During straight-walking trials, the biped's FSR sensors and Roll/Pitch/Yaw angles revealed a periodic load transfer between the anterior and posterior sections of the tail (Figs. 10 and 11). This pattern indicates that the tail functions as an active stabilizing limb rather than a passive appendage, consistent with the tail repositioning phase observed in kangaroo pentapedal locomotion [13]. The FSR measurements show that the tail effectively converts the system into a tripedal support configuration, enabling stable locomotion on flat terrain. During experiments, the compliant continuum legs were only able to support the robot's weight when sharing the load, highlighting the tail's essential role in maintaining balance and enabling forward motion. These observations provide direct evidence that the active tail contributes dynamically to locomotor stability as a load-bearing limb, and the FSR and IMU feedback are shown in Figs. 10 and 11, respectively

Continuum structures inherently exhibit limited load-bearing capacity under compression and are susceptible to deformation and buckling. Prior studies have shown that elastic instability and buckling arise in continuum robots

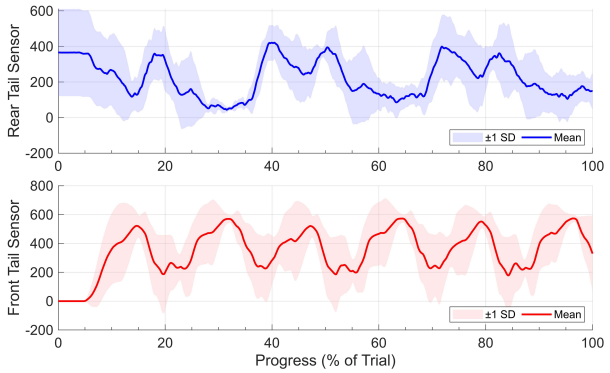


Fig. 10. Average ensemble and ± 1 standard deviation of tail rear (top) and front (bottom) FSR across 4 straight walking trials. FSR data during 4 straight walking trials. Signals are normalized to 0% to 100% with a 0.1 s moving average window.

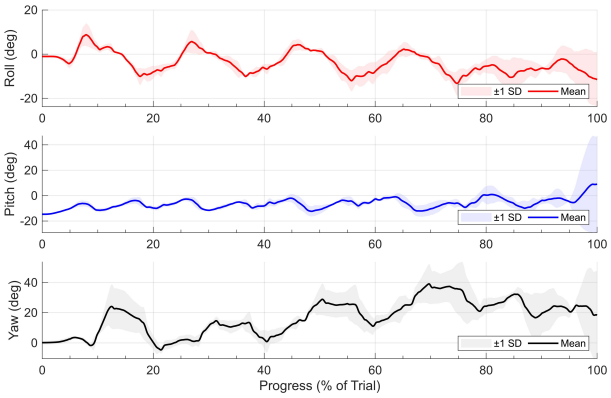


Fig. 11. Mean and ± 1 standard deviation of roll, pitch, and yaw over multiple trials of 60 seconds straight-line walking.

subjected to axial loads [32]. While previous work has emphasized compliance in continuum-legged systems, the present results demonstrate that reducing the number of supporting legs increases the likelihood of structural buckling. The active tail mitigates this failure mode by providing a critical third point of support, supporting the hypothesis that compliant continuum bipeds benefit from auxiliary load-bearing structures.

TABLE I

WORK DONE AND TILT ANGLES ACROSS TERRAINS (MEAN ± STANDARD DEVIATION).

| Terrain | Work (J) | Lateral (°) | Forward (°) |
|---|---|---|---|
| Flat | $509.83 \pm 152.11$ | $7.02 \pm 4.91$ | $8.53 \pm 4.51$ |
| Grass | $367.15 \pm 4.64$ | $4.89 \pm 3.02$ | $4.65 \pm 2.49$ |
| Obstacle | $351.08 \pm 110.68$ | $6.23 \pm 4.07$ | $4.99 \pm 2.99$ |

Uneven-terrain trials further illustrate the tradeoff between stability and locomotion speed. As summarized in Table I, flat ground walking produced the highest mechanical work and disturbance levels, as the biped maintained continuous forward motion without interrupting its gait. In contrast, grass and obstacle trials required intermittent activation of vaulting and yaw controllers, reducing forward progress and overall work. This may be due to the increased friction forces between the biped's foot and the environment that facilitate easier clearance. These behaviors also limited vertical body motion, resulting in reduced forward tilt (i.e., pitch) as shown in Fig. 12. While reflexive gait modulation improves stability on uneven terrain, it comes at the cost of reduced locomotion speed, highlighting a fundamental tradeoff in continuum-based legged robot design.

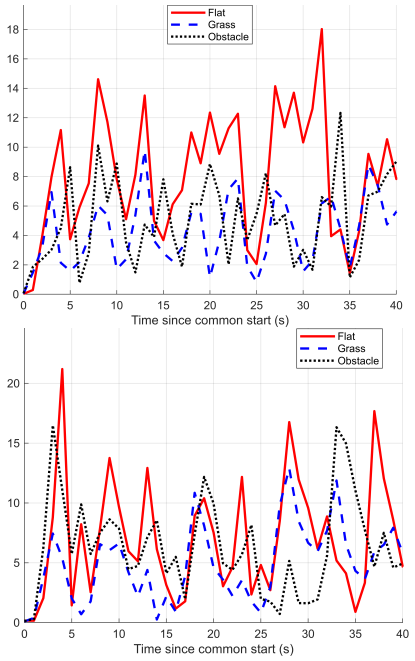


Fig. 12. Averaged pitch (top) and roll (bottom) angles of the biped traversing through different terrains.

### B. Navigation and Obstacles Avoidance Trials

The average power consumption of 7 trials of obstacle avoidance is shown in Fig. 13. The average time it took for a trial to be completed was 276.8 seconds, and the average energy usage was 2173.4 joules and 0.6 watt-hours. The average power used across all seven trials was 7.85 Watts.

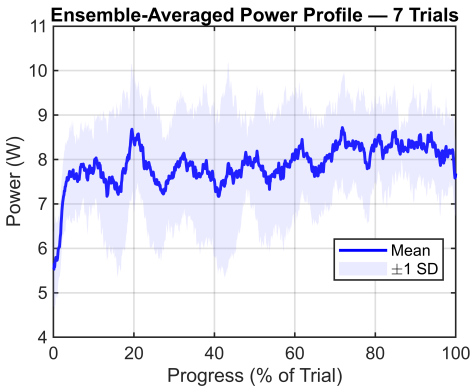


Fig. 13. Ensemble-averaged and ±1 · standard deviation power across all seven trials of obstacle avoidance.

### C. Push Recovery under External Perturbations

Following data collection for both back and lateral collision trials, the signals were refined for analysis. A 0.5 Hz high-pass filter and a 6 Hz low-pass filter were applied to mitigate drift and sensor noise from the BNO080 IMU, followed by a 200 ms Savitzky-Golay filter for additional smoothing. To isolate the primary perturbation response, analysis was restricted to a 10-14 second time window. The displacement trajectory was treated as a spatial curve, and its arc length was computed to quantify total motion during the perturbation. Orientation data were transformed from body to world frames to compute the sensor's vertical axis relative to gravity. Together, the arc-length and orientation-based metrics provide quantitative measures of push-recovery performance, which are summarized in Tables II to IV.

TABLE II

SIDE PERTURBATION DISPLACEMENT BASED ON ACCELERATION

| | Acceleration-based [m] | | |
|---|---|---|---|
| Trial | Steady | No Recovery | With Recovery |
| 1 | 0.007 | 0.255 | 0.180 |
| 2 | 0.010 | 0.286 | 0.257 |
| 3 | 0.014 | 0.270 | 0.208 |
| 4 | 0.009 | 0.321 | 0.216 |
| 5 | 0.010 | 0.426 | 0.240 |
| Average | $0.010 \pm 0.003$ | $0.312 \pm 0.069$ | $0.220 \pm 0.030$ |

TABLE III

BACK PERTURBATION DISPLACEMENT BASED ON ACCELERATION

| | Acceleration-based [m] | | |
|---|---|---|---|
| Trial | Steady | No Recovery | With Recovery |
| 1 | 0.013 | 0.333 | 0.280 |
| 2 | 0.013 | 0.306 | 0.243 |
| 3 | 0.012 | 0.462 | 0.222 |
| 4 | 0.014 | 0.357 | 0.237 |
| 5 | 0.010 | 0.347 | 0.204 |
| Average | $0.012 \pm 0.001$ | $0.361 \pm 0.059$ | $0.237 \pm 0.028$ |

TABLE IV

BACK PERTURBATION DISPLACEMENT BASED ON ORIENTATION. PEAK ARC IS COMPUTED FROM TILT WITH SENSOR RADIUS $R = 0.175$ m.

| | Orientation-based [m] | | |
|---|---|---|---|
| Trial | Steady | No Recovery | With Recovery |
| 1 | 0.000 | 0.218 | 0.032 |
| 2 | 0.000 | 0.214 | 0.056 |
| 3 | 0.000 | 0.221 | 0.057 |
| 4 | 0.000 | 0.221 | 0.062 |
| 5 | 0.000 | 0.222 | 0.049 |
| Average | $0.000 \pm 0.000$ | $0.219 \pm 0.003$ | $0.051 \pm 0.012$ |

The pendulum experiments demonstrate the continuum leg's ability to tolerate and reject external disturbances. In side-collision trials, the mean acceleration-based displacement decreased by 29.5%, from 0.312 m during collision without recovery to 0.220 m with active recovery enabled. Similar trends were observed in back-push experiments, with displacement reductions of 76% for orientation-based metrics and 34% for acceleration-based metrics. In all cases, the recovery condition exhibited substantially lower displacement amplitudes than the no-recovery impact trials. The theoretical arc length corresponding to a complete tip-over is 0.275 m; comparison with both acceleration- and orientation-based estimates provides insight into the accuracy and conservatism of the displacement metrics.

TABLE V

SPEED COMPARISON OF TAILED, AQUATIC, AND MULTILEGGED ROBOTS

| Category | Robot | Speed (mm/s) | Legs | Actuation |
|---|---|---|---|---|
| Tailed | Mudskipper [33] | 69.0 | 2+Tail | Electric |
| | Our prototype | 5.08 | 2+Tail | Electric |
| | Buckley [34] | 50.0 | 4+Tail | Electric |
| Aquatic | Wu [35] | 64.8 | 2 | Electric |
| | Hexapus [36] | 3.4 | 6 | Electric |
| Multilegged | Liang [17] | 100.0 | 4 | Electric |
| | Drotman [21] | 15.57 | 4 | Pneumatic |
| | Liu [19] | 101.0 | 6 | Pneumatic |

Finally, Table V summarizes the locomotion speed, leg count, tail configuration, and actuation method for similar robots. Pneumatic actuation can generate high force and payload capacity, as demonstrated by Drotman et al. in [20], but typically requires offboard air supply or heavy onboard regulation hardware. Fully onboard pneumatic systems, such as the second-generation continuum robot in [21], integrate a $CO_2$ canister but remain limited in maneuverability, exhibiting primarily straight-line locomotion and simple obstacle avoidance. Moreover, pneumatic continuum legs are susceptible to buckling under increased loads, which becomes more pronounced as onboard air storage and regulation hardware add mass.

In contrast, our prototype employs fully onboard electric actuation, enabling all sensing, control, and power components to be integrated on a local microcontroller without tethers, thereby avoiding constraints on the operational workspace. Although quadrupedal and hexapedal robots generally achieve higher speeds than the proposed prototype, which is a trend consistent with biological locomotion-electric actuation provides improved robustness and autonomy. Aquatic bipeds [35], [37] benefit from buoyancy and hydrodynamic effects that enable higher speeds and enhanced stability. Notably, the proposed prototype achieves higher locomotion speed than the Hexapus platform while maintaining full onboard autonomy. Overall, this comparison highlights the trade-offs among actuation strategies and demonstrates the prototype's competitive performance within its design constraints.

## V. CONCLUSIONS

This paper explores the capabilities of a continuum-legged biped equipped with an active, kangaroo-inspired tail. Exper-

iments demonstrate straight-line walking, obstacle avoidance, locomotion over uneven terrain, and pendulum-induced push recovery. Across all scenarios, the robot maintained balance and directional control, and FSR measurements confirm that the tail provides load-bearing stabilization during gait. Future work will increase gait speed and dynamic range through upgraded side-actuation hardware and will investigate reinforcement learning to improve gait adaptation to more complex terrain conditions.

## REFERENCES


[1] A. Mahapatra, S. S. Roy, and D. K. Pratihar, "Multi-legged robots—a review," *Multi-body Dynamic Modeling of Multi-legged Robots*, pp. 11–32, 2020.

[2] P.-B. Wieber, R. Tedrake, and S. Kuindersma, "Modeling and control of legged robots," in *Springer handbook of robotics*. Springer, 2016, pp. 1203–1234.

[3] C. A. D. Bezerra and D. E. Zampieri, "Biped robots: The state of art," in *International Symposium on History of Machines and Mechanisms: Proceedings HMM2004*. Springer, 2004, pp. 371–389.

[4] H. Geyer, A. Seyfarth, and R. Blickhan, "Compliant leg behaviour explains basic dynamics of walking and running," *Proceedings of the Royal Society B: Biological Sciences*, vol. 273, no. 1603, pp. 2861–2867, 2006.

[5] P. M. Wensing, A. Wang, S. Seok, D. Otten, J. Lang, and S. Kim, "Proprioceptive actuator design in the MIT cheetah: Impact mitigation and high-bandwidth physical interaction for dynamic legged robots," *IEEE Transactions on Robotics*, vol. 33, no. 3, pp. 509–522, 2017.

[6] C. Hubicki, A. Abate, P. Clary, S. Rezazadeh, M. Jones, A. Peekema, J. Van Why, R. Domres, A. Wu, W. Martin, H. Geyer, and J. W. Hurst, "Walking and running with passive compliance: Lessons from engineering a live demonstration of the ATRIAS biped," *IEEE Robotics & Automation Magazine*, vol. 25, no. 3, pp. 23–39, 2018.

[7] M. Calisti, G. Picardi, and C. Laschi, "Fundamentals of soft robot locomotion," *Journal of The Royal Society Interface*, vol. 14, no. 130, p. 20170101, 2017.

[8] I. S. Godage, T. Nanayakkara, and D. G. Caldwell, "Locomotion with continuum limbs," in *2012 IEEE/RSJ International Conference on Intelligent Robots and Systems (IROS)*, 2012.

[9] C. L. Huffard, F. Boneka, and R. J. Full, "Underwater bipedal locomotion by octopuses in disguise," *Science*, vol. 307, no. 5717, p. 1927, Mar. 2005.

[10] C. L. Huffard, "Locomotion by abdopus aculeatus (cephalopoda: Octopodidae): walking the line between primary and secondary defenses," *J. Exp. Biol.*, vol. 209, no. 19, pp. 3697–3707, Oct. 2006.

[11] P. Amodio, L. Borrelli, and G. Fiorito, "Bipedal locomotion in octopus vulgaris: A complementary observation," *Ecol. Evol.*, vol. 11, no. 8, pp. 3720–3723, Apr. 2021.

[12] N. Ozkaya, T. Speck, M. S. Fischer, and R. Blickhan, "The kangaroo's tail propels and powers pentapedal locomotion," *Biol. Lett.*, vol. 11, no. 11, p. 20150704, Nov. 2015.

[13] R. S. Dawson, N. M. Warburton, H. L. Richards, and N. Milne, "Walking on five legs: investigating tail use during slow gait in kangaroos and wallabies," *Aust. J. Zool.*, vol. 63, no. 3, pp. 192–200, Jul. 2015.

[14] R. Dawson, N. Milne, and N. M. Warburton, "Muscular anatomy of the tail of the western grey kangaroo, macropus fuliginosus," *Aust. J. Zool.*, vol. 62, no. 2, pp. 166–174, Apr. 2014.

[15] I. Godage, D. T. Branson, E. Guglielmino, and D. G. Caldwell, "Locomotion with continuum limbs," in *Proc. Int. Conf. Intell. Robots Systs.*, 2012, pp. 293–298.

[16] I. D. Walker and A. Mutlu, "Continuum robots for space applications," in *Proceedings of the IEEE Aerospace Conference*, 2012, pp. 1–11.

[17] A. Ji, J. Liang, H. Chen, and J. S. Dai, "Reinforcement learning for quadruped continuum actuators," *Soft Rob.*, vol. 9, no. 3, pp. 456–467, 2022.

[18] V. Muralidharan, P. Krishna, T. G. Thuruthel, and F. Iida, "A soft quadruped robot enabled by continuum actuators," *IEEE Rob. Autom. Lett.*, vol. 6, no. 2, pp. 2270–2277, 2021.

[19] Z. Liu and N. Lu, "Sorx: A soft pneumatic hexapod robot on rough, steep, and unstable terrain," *Soft Rob.*, vol. 7, no. 5, pp. 597–608, 2020.

[20] D. Drotman, S. Jadhav, M. Karimi, P. deZonia, and M. T. Tolley, "3d printed soft actuators for a legged robot capable of navigating unstructured terrain," in *Proceedings of the IEEE Int. Conf. Robot. Autom.*, 2017, pp. 5532–5539.

[21] D. Drotman, S. Jadhav, D. Sharp, C. Chan, and M. T. Tolley, "Electronics-free pneumatic circuits for controlling soft-legged robots," *Sci. Rob.*, vol. 6, no. 50, p. eaay2627, 2021.

[22] M. Verma, A. Ainla, D. Yang, and G. M. Whitesides, "A soft tube climbing robot," *Proceedings of the National Academy of Sciences USA*, vol. 115, no. 28, pp. 7126–7131, 2018.

[23] L. Qin, Z. Xu, T. Li, and H. Ren, "A versatile soft crawling robot with rapid locomotion," *Soft Rob.*, vol. 6, no. 3, pp. 333–345, 2019.

[24] E. Joyee and C.-H. Pan, "A fully three-dimensional printed inchworm-inspired soft robot with magnetic actuation," *Soft Rob.*, vol. 6, no. 3, pp. 333–345, 2019.

[25] J. Zou, Y. Lin, C. Ji, and H. Yang, "A reconfigurable omnidirectional soft robot based on caterpillar locomotion," *Soft Rob.*, vol. 5, no. 2, pp. 164–174, 2018.

[26] W. Liu, T. Wang, and J. Zhang, "A bio-inspired hopping kangaroo robot with an active tail," *Bioinspiration & Biomimetics*, vol. 9, no. 4, p. 046008, 2014.

[27] H. An, Y. Kim, and S. Lee, "Development of a bipedal hopping robot with a morphable inertial tail for agile locomotion," *IEEE Rob. Autom. Lett.*, vol. 5, no. 3, pp. 4457–4464, 2020.

[28] W. S. Rone and P. Ben-Tzvi, "Continuum robotic tail loading analysis for mobile robot stabilization and maneuvering," in *International design engineering technical conferences and computers and information in engineering conference*, vol. 46360. American Society of Mechanical Engineers, 2014, p. V05AT08A009.

[29] E. A. Lee and S. A. Seshia, *Introduction to Embedded Systems: A Cyber-Physical Systems Approach*, 2nd ed. Berkeley, CA, USA: MIT Press, 2017.

[30] R. Tedrake, "Underactuated robotics: Algorithms for walking, running, swimming, flying, and manipulation," MIT OpenCourseWare, Cambridge, MA, USA, 2023.

[31] S. Monteleone, F. Negrello, G. Grioli, M. G. Catalano, A. Bicchi, and M. Garabini, "A method to benchmark the balance resilience of robots," *Front. Rob. AI*, vol. 9, p. 817870, 2023.

[32] C. D. Rucker, B. A. Jones, and R. J. Webster III, "A geometrically exact model for externally loaded concentric-tube continuum robots," *IEEE Trans. Rob.*, vol. 26, no. 6, pp. 769–780, Dec. 2010.

[33] J. Buckley, N. Chikere, and Y. Ozkan-Aydin, "The effect of tail stiffness on a sprawling quadruped locomotion," *Front. Rob. AI*, vol. 10, p. 1198749, 2023.

[34] S. Liu, M. Sagare, S. Patil, and F. Qian, "Bio-inspired tail oscillation enables fast crawling on deformable granular terrains," *arXiv*, 2025.

[35] X. Wu, H. Li, and K. Wang, "Coconut octopus inspired underwater bipedal walking robot," *Bioinspiration & Biomimetics*, vol. 17, no. 3, p. 036002, 2022.

[36] Q. Yu and N. Gravish, "Multimodal locomotion in a soft robot through hierarchical actuation," *Soft Rob.*, vol. 11, no. 1, pp. 21–31, 2024.

[37] X. Wu, H. Li, and K. Wang, "Hybrid underwater locomotion in an octopus-inspired continuum robot," *Nature Communications*, vol. 15, p. 4947, 2024.